Engineering Geology 297 (2022) 106498

Contents lists available at ScienceDirect

Engineering Geology

journal homepage: www.elsevier.com/locate/enggeo

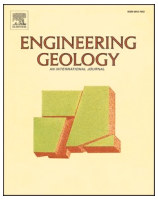

Investigation of shallow S-wave velocity structure and site response parameters in Taiwan by using high-density microtremor measurements

Chun-Te Chen [a], Chun-Hsiang Kuo [b,c,d,*], Che-Min Lin [d], Jyun-Yan Huang [d], Kuo-Liang Wen [e]

[a] Disaster Prevention Technology Research Center, Sinotech Engineering Consultants (Inc.), Taipei, Taiwan, ROC
[b] Department of Earth Sciences, National Central University, Taoyuan, Taiwan, ROC
[c] Earthquake-Disaster & Risk Evaluation and Management Center, National Central University, Taoyuan, Taiwan, ROC
[d] National Center for Research on Earthquake Engineering, Taipei, Taiwan, ROC
[e] Department of Earth Sciences, National Central University, Taoyuan, Taiwan, ROC

ARTICLE INFO

Keywords:
Shallow S-wave velocity
Diffuse field theory
Microtremor
HVSR
V_{S30},$Z_{1.0}$

ABSTRACT

Site effect is considered a critical component affecting ground motions, and the shallow velocity structure is a primary factor for determining the site effect. The shallow velocity structure should be carefully evaluated to mitigate earthquake hazards. Thus, we use microtremor array measurements as well as the inversion of microtremor horizontal-to-vertical spectral ratios (MHVSRs) to investigate shallow S-wave velocity (Vs) profiles in Taiwan, which is one of the most seismically active areas of the world. On the basis of the diffuse field assumption, Vs profiles can be efficiently inverted. To reduce the nonuniqueness of MHVSR inversion, Vs profiles obtained using microtremor array measurements and from an engineering geological database were adopted as model constraints. Finally, this study included 3587 inverted MHVSR Vs profiles and 65 inverted Vs profiles from microtremor arrays. The results were used to create a detailed updated V_{S30} map of Taiwan and to map the depth contours of $Z_{1.0}$; thus, the relationship between V_{S30} and $Z_{1.0}$ was determined. We proposed a new parameter, H_R, as a proxy for V_{S30}, that is defined as a ratio of the average MHVSR across high- and low-frequency bands. This parameter was correlated to the predominant frequency without subjective selection. Moreover, we constructed a pseudo-three-dimensional shallow Vs model of Taiwan, which describes main shallow structural features and provides complete details for plain areas.

1. Introduction

Site effect is considered an essential factor affecting earthquake ground motion and the resulting earthquake damage distribution (Guéguen et al., 1998; Panou et al., 2005; Singh et al., 1988). The shallow velocity structure is a primary factor for the evaluation of the site effect. Obtaining information regarding the underground structure for velocity distribution is vital for understanding the characteristics of earthquake ground motion, especially in sedimentary environments.

Several conventional methods, including invasive and noninvasive approaches, have been used to investigate the shallow velocity structure. The suspension PS logging test (Kaneko et al., 1990; Ogura, 1988) is an invasive method used for determining P-wave velocity and S-wave velocity (Vs) through velocity logging. Although this method can reliably measure propagation velocities through layers (Kaneko et al., 1990), it is expensive. Furthermore, obtaining land use permits for borehole drilling is difficult, especially in urban areas.

A low-cost tool has been established to estimate the shallow Vs structure (Horike, 1985; Matsushima and Okada, 1990; Tokimatsu et al., 1992) based on an engineering seismology technique using microtremor array records. This noninvasive method does not adversely affect the environment and can be deployed anywhere, even in urban areas. Moreover, deeper Vs structures can be estimated by increasing the array aperture. Hence, to investigate the shallow Vs structure, this procedure has been more widely adopted than active source techniques, such as the spectral analysis of surface waves (Nazarian et al., 1983) and multichannel analysis of surface waves (Park et al., 1999), especially in populated areas.

Subduction and collision processes in the Eurasia plate and Philippine Sea plate resulted in the formation of Taiwan's complex geological

* Corresponding author at: No. 300, Zhongda Rd., Zhongli District, Taoyuan City 320317, Taiwan, ROC.
E-mail addresses: pokayoke@sinotech.org.tw (C.-T. Chen), chkuo@ncu.edu.tw (C.-H. Kuo), cmlin@narlabs.org.tw (C.-M. Lin), jyhuang@narlabs.org.tw (J.-Y. Huang), wenkl@cc.ncu.edu.tw (K.-L. Wen).

https://doi.org/10.1016/j.enggeo.2021.106498
Received 1 April 2021; Received in revised form 7 December 2021; Accepted 8 December 2021
Available online 11 December 2021

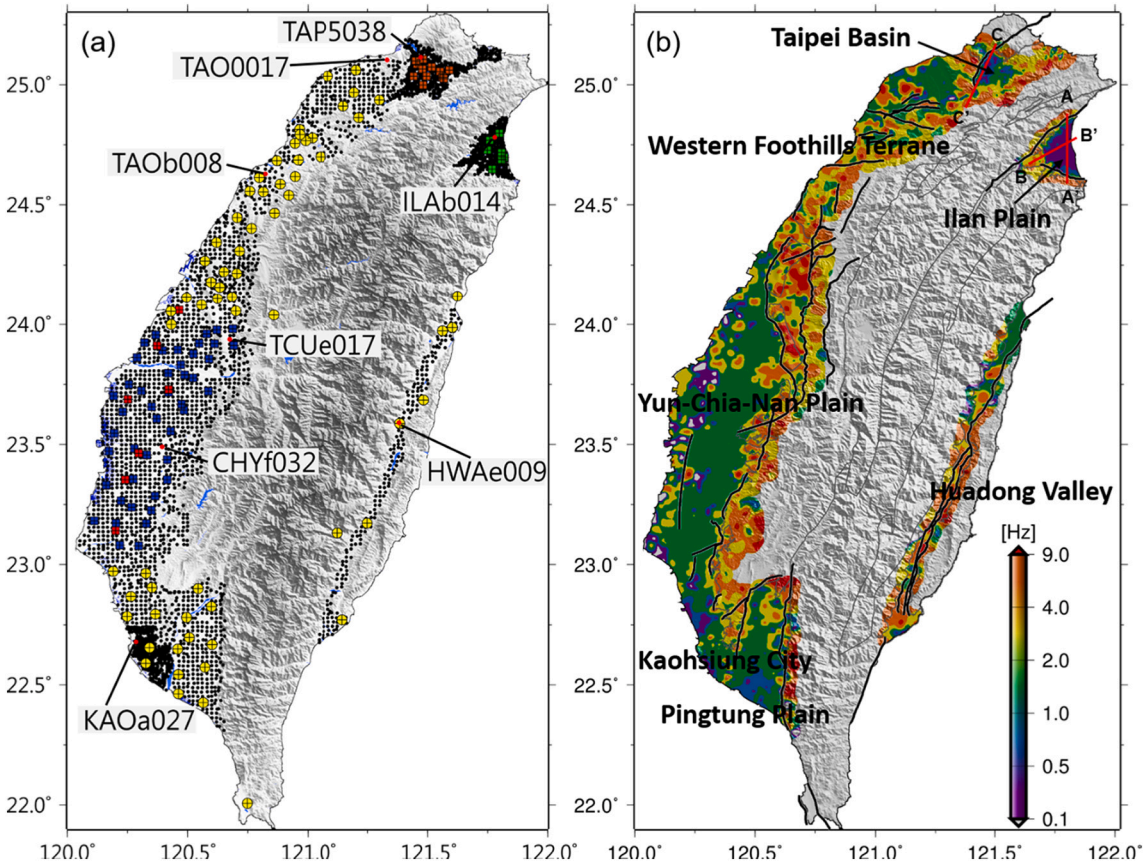

Fig. 1. (a) Location of dense microtremor survey sites in Taiwan. The black dots represent single-station survey sites, which have measurement intervals of 1 km for the Taipei Basin, Ilan Plain, and Kaohsiung City and 2 km for other areas. The yellow circles represent microtremor array measurements from this study. The green, brown (Kuo, 2004), blue, and red (Kuo et al., 2016) squares indicate the locations of microtremor arrays presented in previous studies. (b) The predominant frequency (f_{peak}) contour map in Taiwan (Wen and Huang, 2012). The black lines denote the 38 major seismogenic structures (Shyu et al., 2016) of Taiwan. (For interpretation of the references to colour in this figure legend, the reader is referred to the web version of this article.)

island structure with a series of faults and folds and high seismicity. The Taiwan Earthquake Model (TEM) project established a probabilistic seismic hazard map (named TEM PSHA2015) (Wang et al., 2016) of Taiwan. The map revealed that expected peak ground acceleration can be higher than 0.5 g in the southwestern plains, Hengchun, and the Longitudinal Valley. However, the TEM PSHA2015 did not consider the site effect; the model represented seismic hazards for engineering bedrock (V_{S30} = 760 m/s) at all sites, where V_{S30} is the average Vs for a depth of 30 m. In the new version of the seismic hazard model of Taiwan, the TEM PSHA2020 (Chan et al., 2020), site amplification was assessed on the basis of V_{S30} at 816 sites collected from the engineering geological database of the Taiwan Strong Motion Instrumentation Program (EGDT, http://egdt.ncree.org.tw/). This assessment indicated that the site effect considerably affects the seismic hazard, resulting in a higher hazard level than that in the previous model in the Taipei Basin, Ilan Plain, and Yun–Chia–Nan Plain. This finding demonstrates the importance of the site effect, which should be considered for ground-motion evaluations. On the basis of the numerical modeling of three-dimensional (3D) seismic waves, some studies (Chen et al., 2016; Lee et al., 2008; Miksat et al., 2010) have investigated the seismic wave amplification of subsurface structures in Taiwan and indicated that shallow low-velocity formations can significantly amplify seismic waves. A detailed shallow velocity structure can provide essential information for engineering purposes and facilitate the development of a 3D velocity model for ground motion simulation to mitigate earthquake damage.

Since 2000s, many studies have performed microtremor array measurements to investigate shallow Vs structures in Taiwan (Huang and Wu, 2006; Huang et al., 2015; Kuo et al., 2009, 2016; Lin et al., 2009; Satoh et al., 2001; Wu and Huang, 2012, 2013). The microtremor array method is believed to be a reliable and useful tool for estimating shallow Vs structures. These studies have provided valuable Vs profiles for evaluating the site effect, mapping engineering bedrock, and understanding depositional processes. However, these studies have focused only on particular small areas. Moreover, microtremor array measurements cannot be used to perform sufficiently dense surveys covering all the plain areas of Taiwan uniformly because of economic, human resource, and spatial limitations. Hence, the Vs profiles reported by previous studies are inadequate for mapping engineering bedrock or constructing 3D velocity models at a scale appropriate for the entire Taiwan.

A denser survey can be performed using single-station microtremor measurements than microtremor array measurements, especially in a metropolitan area such as Taipei City. A project deployed approximately 4000 single-station microtremor survey points around the plains, basins, and foothills of Taiwan. The spatial distribution of horizontal survey points reached approximately 1 km in urban areas and 2 km in other areas. A study performed microtremor horizontal-to-vertical spectral ratio (MHVSR) analysis based on dense microtremor survey data to investigate the site effect in Taiwan (Wen and Huang, 2012). The diffuse field assumption (DFA) approach has been developed (García-Jerez et al., 2013; Kawase et al., 2011; Sánchez-Sesma et al., 2011) to interpret the theory of MHVSR and obtain the shallow velocity structure (García-Jerez et al., 2016) based on the MHVSR inversion technique. High-density velocity profiles in Taiwan can be obtained using this inversion technique with microtremor data.

In this study, we estimated Vs structures in high-density spatial

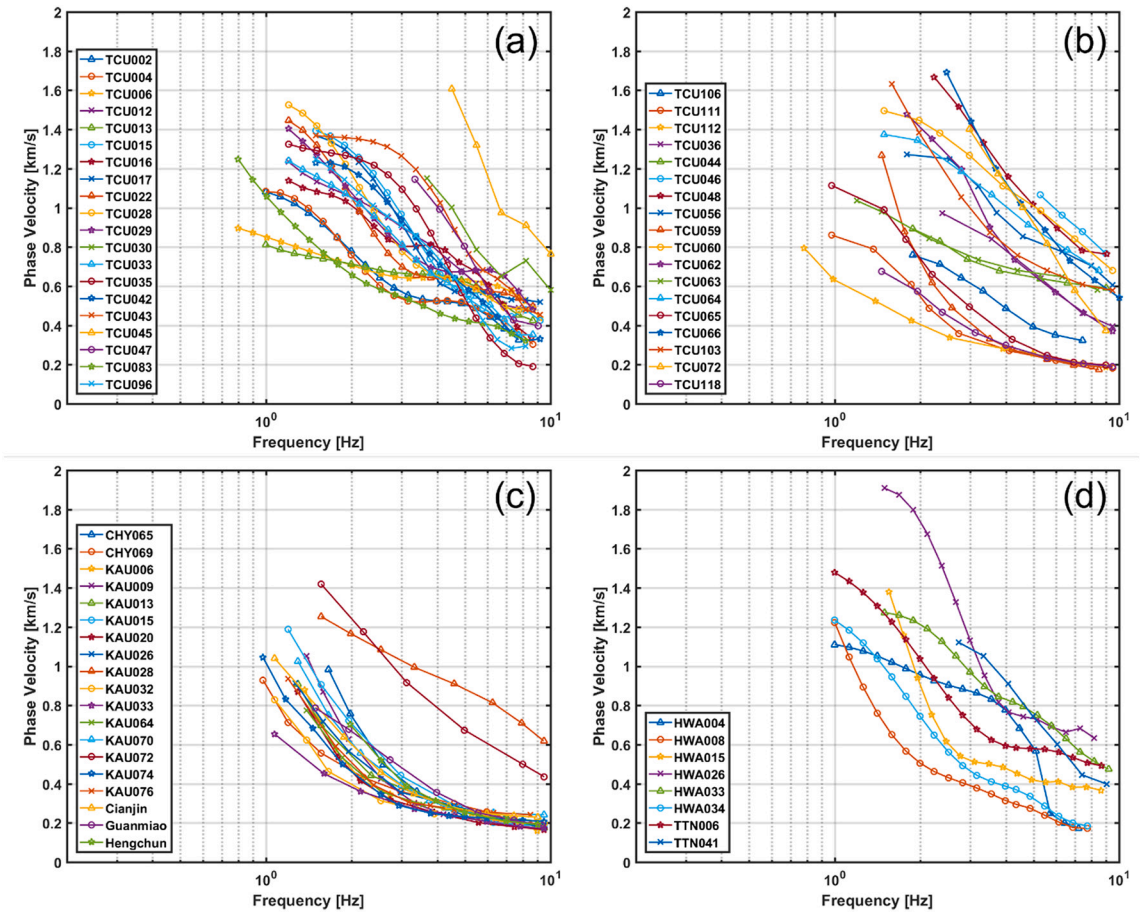

Fig. 2. Phase velocities obtained from the array measurements in this study by applying the F–K method at 65 microtremor array sites. For readability, the sites are divided into four panels.

distributions for all the plain areas of Taiwan through two main steps. First, microtremor array measurements in the Western Foothills Terrane, Pingtung Plain, and Huadong Valley were collected. On the basis of high-resolution frequency–wavenumber (F–K) analysis (Capon, 1969), the Rayleigh wave dispersion curves were estimated. Subsequently, the surface wave inversion technique was applied to obtain Vs profiles. Second, we adopted the MHVSR inversion technique based on the DFA to investigate shallow Vs structures. More than 3500 one-dimensional (1D) Vs profiles were obtained in this study; these profiles can provide useful information for establishing a detailed velocity model for numerical seismic wave simulations and help determine valuable engineering earthquake parameters such as V_{S30}, $Z_{1.0}$ (a depth parameter defining the depth in meters where Vs is 1.0 km/s), and engineering bedrock.

Several studies (Hassani and Atkinson, 2016; Karagoz et al., 2015; Yilar et al., 2017; Yaghmaei-Sabegh and Hassani, 2020) have used the predominant frequency of the MHVSR or earthquake horizontal-to-vertical spectral ratio (EHVSR) to determine the relationship between local geological conditions (V_{S30}) and the MHVSR or EHVSR. Wald and Allen (2007) reported that V_{S30} well-correlated with the topographic slope, which is the maximum elevation gradient at each point. Many studies have since adopted the digital elevation model (DEM) or geotechnical categories to develop a proxy for V_{S30} (Ancheta et al., 2013; Seyhan et al., 2014). Kwok et al. (2018) demonstrated regional proxy relationships in Taiwan used for V_{S30} prediction, and Heath et al. (2020) developed a global slope-based V_{S30} map. In addition, we applied our inverted V_{S30} database and MHVSRs to develop a new relationship between V_{S30} and the MHVSR through our proposed parameter, H_R, and elevation. The parameter H_R is a ratio of the average MHVSR across high-frequency bands to that across low-frequency bands; it can be easily calculated and demonstrates a favorable V_{S30} prediction ability. This parameter allowed us to rapidly evaluate V_{S30}values with high accuracy for sites by using MHVSRs.

2. Data

The main purpose of this study was to obtain a dense map of shallow Vs structures in Taiwan. Several types of measurement data were used to develop this map. First, the single-station microtremor survey included 3789 survey points uniformly distributed around the plains, basins, and foothills of Taiwan. Microtremor data were recorded using the 24-bit digital recorder SAMTAC-801B and the triaxial-servo velocity sensor VSE-311C or VSE-315D (Tokyo Sokushin) with a flat amplitude response at 0.1–70 Hz. Each single-station microtremor survey included 18 min of recordings at a sampling rate of 200 Hz. The method used by Nakamura (1989) with a time window length of 8192 points was applied to all the recordings to obtain MHVSRs and investigate the site effect throughout Taiwan (Wen and Huang, 2012). Furthermore, the processed data were used to obtain shallow Vs structures by applying the MHVSR inversion technique.

Velocity profiles from 136 microtremor arrays were used to design suitable velocity and thickness search ranges for each MHVSR site near the deployed array location to overcome the nonuniqueness problem. Among the 136 microtremor arrays, 71 have been reported in previous studies (Kuo, 2004; Kuo et al., 2009; Kuo et al., 2016; Lin et al., 2009), and these arrays mostly cover the Taipei Basin, Ilan Plain, and Yun–Chia–Nan Plain areas. In addition, microtremor array measurements were performed at 65 sites that were generally uniformly distributed

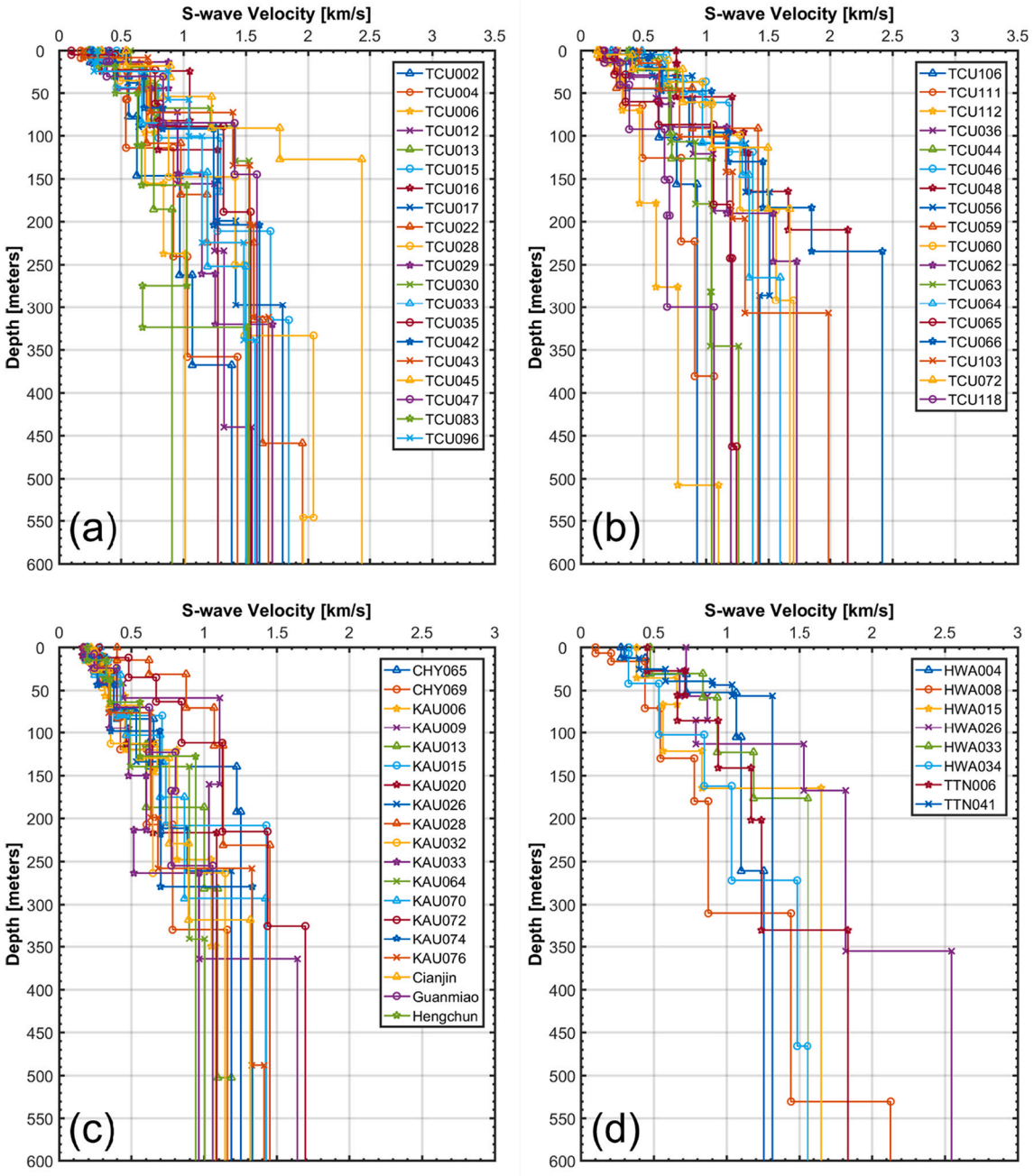

Fig. 3. Inverted Vs structures at 65 sites obtained in this study.

around the other areas in this study. Fig. 1a displays the locations of the dense microtremor survey points in the plain regions of Taiwan. In addition, microtremor array measurement locations are presented in the same figure. Fig. 1b shows the MHVSR predominant frequency (f_{peak}) contour map in Taiwan (Wen and Huang, 2012). Finally, we used site parameters, namely V_{S30} and $Z_{1.0}$, from the EGDT (Kuo et al., 2011, 2012) to validate the resulting model obtained using the MHVSR inversion technique.

3. Methodology

3.1. Inversion of the microtremor array measurement dispersion curve

In this study, the Rayleigh wave phase velocity dispersion curve from each array measurement site was estimated by performing high-resolution F–K spectral analysis on the basis of the maximum likelihood method (MLM) proposed by Capon (1969). The MLM uses cross-power spectral densities to estimate the F–K spectrum. The cross-power spectral densities $P(f,k)$ can be expressed as

$$P\left(f,\vec{k}\right)=\left\{\sum_{n,m=1}^{N}\varnothing_{nm}^{-1}(f)\bullet exp\left[i\vec{k}\bullet\left(\vec{X}_n-\vec{X}_m\right)\right]\right\}^{-1} \quad (1)$$

where f is the frequency; $\vec{k}$ is the two-dimensional horizontal wavenumber vector; $i=\sqrt{-1}$; N is the number of sensors; $\varnothing_{nm}{}^{-1}(f)$ is the corresponding element of the inverse of the matrix $\varnothing_{nm}$ at frequency f, which is the estimate of the cross-power spectrum between the n_{th} and m_{th} data points; and $\vec{X}_n$ and $\vec{X}_m$ are the position vectors of the n_{th} and m_{th} sensors, respectively.

For the grids of the two cartesian components of the horizontal wavenumber, the F–K spectra were computed at a resolution of 201 ×

201 nodes for each frequency. Phase velocities were calculated from F–K spectral analysis results in the wavenumber domain at each frequency and each wavenumber (k_x, k_y) corresponding to the maximum peak of the F–K spectra. The phase velocity c is given by

$$c = f \Big/ \sqrt{k_{x0}^2 + k_{y0}^2} \tag{2}$$

where k_{x0} and k_{y0} represent the positions of peak power in the wavenumber domain.

Fig. 2 displays the dispersion curves of phase velocities obtained from the array measurements in this study by applying the F–K method. Based on previous experiences (e.g. Satoh et al., 2001), the minimum frequency considered reliable was that corresponding to six times the maximum array separation. Array stations for TCU and HWA (Fig. 2a, b, d) were mostly distributed in the Western Foothills Terrane and Huadong Valley (Fig. 1), which generally have higher and steeper phase velocities than the stations in the Pingtung Plain (Fig. 2c). Hence, the Western Foothills Terrane and Huadong Valley have higher stratum velocities than the Pingtung Plain. In addition, phase velocities can have a diverse range within the same geological area, indicating lateral variations in the understructure.

The genetic algorithm (GA) is a powerful global optimization method that involves the selection, crossover, and mutation of individuals in a population and facilitates the search of an optimal solution both globally and locally (Goldberg, 1989). In this study, we used the GA combined with the forward modeling of surface waves, as proposed by Herrmann (1987), to search for appropriate initial models for all sites within a given search range before the conventional inversion of dispersion curves. A model with eight layers covering a half space was assumed for GA searching and defined both for the velocity and thickness of layers. The full GA process involved conducting 30 GA searches. Each GA search was terminated at the 450th generation. The population size of each generation was 40. Therefore, the total number of repetitions was 540,000 for one complete GA grid search process. Two genetic operations, namely crossover and mutation, were performed to generate populations and prevent localized minimums. The GA was used to search for all possible velocity structures within the given range. The GA program used in this study has been successful implemented in many studies (Kuo, 2004; Kuo et al., 2009; Kuo et al., 2016; Lin et al., 2009). However, the total thickness of layers may be excessive for the estimation of observed dispersion curves. Therefore, after the GA grid search, we inverted the dispersion curves by using the stochastic least-square inversion (Herrmann, 1987) of the fundamental-mode Rayleigh wave to estimate the Vs structures by adopting the initial model provided by the GA grid search. The program SURF proposed by Herrmann (1987) can perform the interactive inversion of surface wave dispersion data. We used this program to test the sensitivities of all layers and exclude false and immaterial layers with insufficient resolutions from the Vs model derived from the GA search step. Subsequently, Vs profiles derived from the GA search step at each site were refined using a conventional surface wave inversion step, which improved the accuracy of the Vs profiles and exhibited the lowest variance. The final Vs structures are divided into four parts in Fig. 3.

3.2. Inversion of MHVSR

The MHVSR method was first proposed by Nakamura (1989) to examine the characteristics of surface ground motions. This low-cost and convenient method produces accurate estimations. Numerous studies have used the MHVSR method to evaluate the site effect or bedrock depth. Subsequently, Nakamura (2019) clarified a few misunderstandings regarding the MHVSR method to ensure its correct application. In this study, we confirmed that the predominant frequency exhibited high consistency with the geological structure; a lower predominant frequency typically indicates an alluvial plain, and foothills or basin edges usually have higher predominant frequencies (Fig. 1b). Nevertheless, a lack of physical theoretical basis has led the MHVSR technique to remain an empirical statement. A physical model is therefore required to more efficiently interpret MHVSR measurements. Sánchez-Sesma et al. (2011) proposed an innovative interpretation that assumes that the seismic field is diffuse. The MHVSR includes all the contributions of Rayleigh, Love, and body waves and can be modeled in terms of the imaginary part of the components of Green's function (GF) for coinciding the source and receiver; this is called the DFA. According to the DFA, the definition of MHVSR is given as follows:

$$\mathrm{MHVSR}(x; w) \equiv \sqrt{\frac{2P_1(x;w)}{P_3(x;w)}} = \sqrt{\frac{2Im[G_{11}(x;x;w)]}{Im[G_{33}(x;x;w)}} \tag{3}$$

The $P_1(x;w)$ is the power spectral densities of motion along the horizontal direction at a point x for frequency equal to $w/2\pi$, whereas $P_3(x;w)$ refers to the vertical degree of freedom. The expressions $P_m(x;w)$ are proportional to the imaginary part of the corresponding GF at the source $G_{mm}(x;x;w)$. The MHVSR can be computed theoretically in terms of Eq. (3) by using the DFA. On the basis of the DFA, the computer code HV-inv (https://w3.ual.es/GruposInv/hv-inv) developed by García-Jerez et al. (2016) was used to obtain velocity profiles through the forward calculation and inversion of MHVSR. Piña-Flores et al. (2017) reported that the forward problem was nonlinear and depended on several uncorrelated parameters. Consequently, several sets of parameters were associated with the same MHVSR. The HV-inv code supports the joint inversion of MHVSRs and dispersion curves and can help mitigate their nonuniqueness.

This study used HV-inv for the forward calculation and inversion of the MHVSR to investigate shallow Vs profiles in Taiwan. To prevent the nonuniqueness of MHVSRs in the forward calculation and inversion process, joint inversion with the dispersion curve was suggested and has been successful in previous studies (Castellaro, 2016; García-Jerez et al., 2019; Picozzi et al., 2005; Senna et al., 2018; Sivaram et al., 2018; Spica et al., 2018; Yamada et al., 2020).

However, dispersion curves are unavailable for most of the single-station microtremor survey locations in this study. Therefore, performing joint inversion to obtain Vs profiles was not feasible in this situation. To mitigate nonuniqueness, suitable velocity and thickness search ranges were designed for each MHVSR individually by considering investigated velocity structures obtained using microtremor array measurements. Microtremor array data were processed and analyzed to obtain Vs profiles in this study. These profiles provide useful velocity information for shallow formations and can contribute to the fields of earthquake engineering and seismological research.

These velocity models were used to design constraints for MHVSR inversion to mitigate the nonuniqueness. A total of 71 microtremor array velocity profiles from previous studies (Kuo, 2004; Kuo et al., 2009, 2016; Lin et al., 2009) were collected to complement the spatial coverage of the survey. In total, we used 136 microtremor array velocity profiles to serve as constraints for MHVSR inversion. We constructed two generic models for "plain" and "piedmont" areas with suitable velocity and thickness ranges. According to the elevation of MHVSR sites, we applied a corresponding generic model as well as the velocity range as the initial model for the inversion. For the setting of searching ranges of inversion, the Vs profiles of nearby microtremor arrays and EGDT were considered, and 4000 inversion models with misfit values were implemented for each MHVSR site. The model range of inversion for a MHVSR site was adjusted, and the inversion was performed again once the misfit exceeded a predefined threshold. Finally, the minimum misfit model was adopted as the final model at a MHVSR site. The procedure of creating initial models with suitable searching ranges for high-density MHVSR inversions depends on sufficient reliable Vs profiles obtained using microtremor arrays and velocity loggings and on the understanding regarding local geology at different regions. Considering that the subsurface structure may vary considerably in particular areas, the upper and lower thickness and velocity bounds for MHVSR inversion

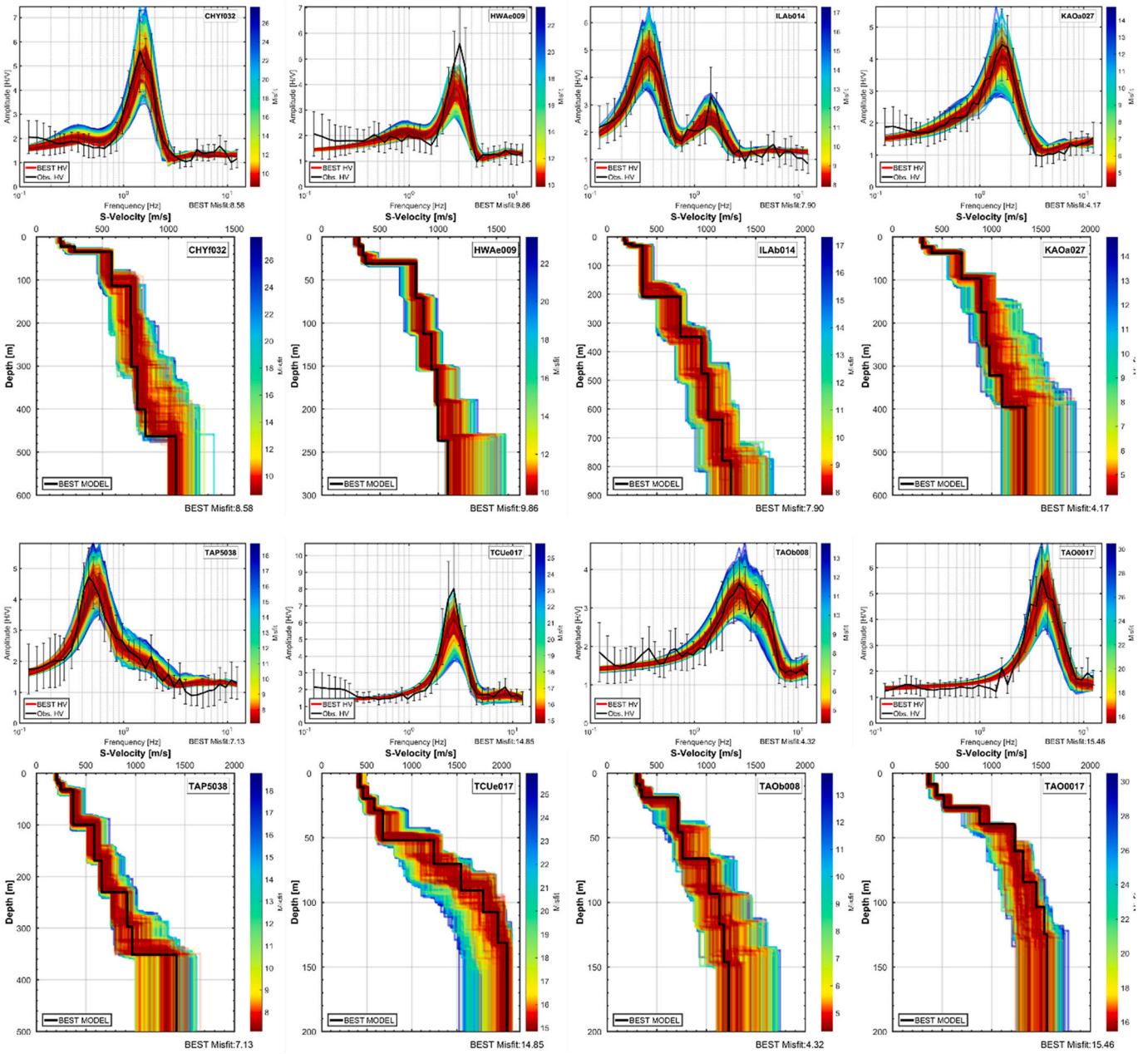

Fig. 4. Examples of MHVSR inversion at eight sites (see locations in Fig. 1a). Top panels display the observed MHVSR (black lines) and its standard deviations, and colored curves are the synthetic MHVSR according to misfit value bars. Bottom panels indicate the best-fitting model (black lines), and the inverted models are colored according to the corresponding misfit value.

were provided in a wide range, particularly for sites with limited constraints due to the large distance from an array site.

Within the suitable ground parameters, the HV-inv program applies the Monte Carlo sampling inversion method to search for the optimal model according to the misfit function, which is defined as

$$misfit(f) = \sum_{i=1}^{n} \frac{\left(d_{fi}^{obs} - d_{fi}^{syn}\right)^2}{\sigma_{fi}^2} \tag{4}$$

where d_f^{obs} is the observed MHVSR at frequency f, d_f^{syn} is the synthetic MHVSR at frequency f, and σ_f is the standard deviation of the observed MHVSR. The lowest misfit value representing the best model was obtained. To speed up the inversion calculation, the observed MHVSRs were downsampled to $n = 37$ and logarithmically equally spaced in the frequency band from 0.12 Hz to 12.4 Hz.

Fig. 4 represents an example of the MHVSR inversion for eight sites from different geological areas. The locations of these sites are indicated in Fig. 1a. The MHVSR inversion mostly had a low misfit value, indicating that this method could be suitable for application to different geological substructures in Taiwan.

4. Results and discussion

In this study, we analyzed microtremor arrays at sites distributed in the Pingtung Plain, Huadong Valley, and Western Foothills Terrane of Taiwan. In addition, we inverted Vs profiles by using the HV-inv program based on the DFA. In the following sections, we discuss the model quality and study results.

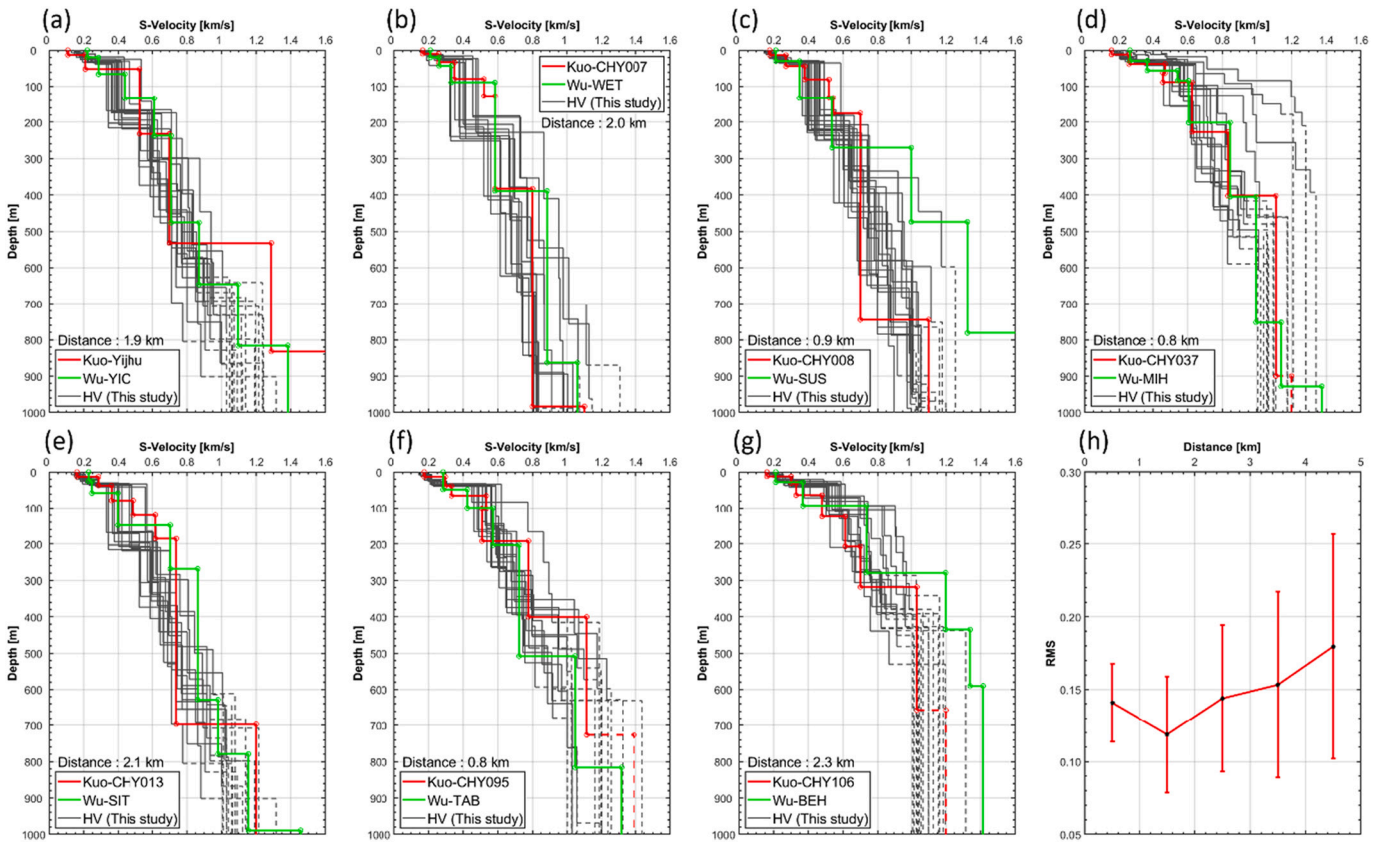

Fig. 5. (a)–(g) Comparison of Vs profiles derived using the microtremor array method and MHVSR inversion in this study. Red and green lines indicate the Vs profiles derived from microtremor array measurements (Kuo et al., 2016; Wu and Huang, 2013). Gray lines are the Vs profiles obtained in this study by using the MHVSR inversion technique at nearby sites. The dashed line denotes the bottom layer of each profile. The distance between the two arrays is illustrated in each figure. (h) Relationship between the Vs difference RMS and distance.

4.1. Model validation

To validate our MHVSR inversion results, additional criteria were applied as thresholds to quantify inversion quality and remove substandard sites. First, we calculated the correlation coefficient (R) between the observed and synthetic MHVSRs for each site. The sites with $R \leq 0.35$ and *misfit* ≥ 40 were removed to ensure that the MHVSR inversion quality was acceptable for each site. Some of the disqualified sites exhibited an abnormal MHVSR, whereas the MHVSRs of other sites were considerably different from those of nearby sites. Those sites might have an extraordinary underground structure (e.g., embedded very-low- or high-velocity layers), which is beyond the designed search range based on microtremor array measurements. A total of 202 sites mostly located near foothill areas did not fulfill the criteria and thus were eliminated from the database. These findings indicated the presence of a complex and varied substructure in Taiwan, especially in the Western Foothills Terrane.

Previous studies have conducted microtremor array measurements in Taiwan to obtain reliable shallow Vs structures (Huang and Wu, 2006; Huang et al., 2015; Kuo et al., 2009, 2016; Lin et al., 2009; Satoh et al., 2001; Wu and Huang, 2012, 2013). The results of some of these studies (Kuo et al., 2009, 2016) were applied in the design of our inversion constraints in this study. To validate our MHVSR inversion results, we compared some Vs profiles with those reported in previous studies obtained using microtremor array measurements. In Fig. 5a–g, the Vs profiles of two array measurements (Kuo et al., 2016; Wu and Huang, 2013) and MHVSR inversions determined in this study are compared. The two previous studies conducted microtremor array measurements at different locations. To ensure the comparability of velocity profiles, we selected only seven arrays with a distance of $\leq$3 km between the arrays. For the MHVSR inversion velocity profiles, we selected sites within 5 km from the arrays reported by Kuo et al. (2016). The results of the comparisons indicated that the MHVSR inversion velocity profiles were in agreement with the microtremor array measurement velocity profiles. This finding demonstrated that a low-cost MHVSR measurement can approximate microtremor array measurements through the use of the DFA inversion technique. We observed significant variations in the velocity structure within a short distance, especially for sites located on a geological boundary (Fig. 5d). In addition, we calculated the root mean square (RMS) of differences between Vs profiles from MHVSRs and the corresponding microtremor arrays from the study conducted by Kuo et al. (2016) for constructing generic Vs models. To calculate the RMS between Vs profiles, we interpolated these Vs profiles into a 10-layer model, with each layer having a uniform thickness of 100 m. The average RMS and standard deviation were obtained for 1-km bins (Fig. 5h). Although the distance between 1 and 2 km had the smallest mean RMS value, the mean and standard deviation of RMS values increased with distance. We speculate that these values can indicate real velocity variations. Hence, a dense survey velocity model for the entire Taiwan is required to obtain more detailed parameters, improve predicted ground motion's accuracy, and mitigate seismic disasters.

4.2. A dense V_{S30} map

V_{S30} is the average Vs at depths of up to 30 m and is a vital site parameter widely used for many purposes such as microzonation, ground motion prediction equations (GMPEs), and building codes (BSSC, 2004; ASCE, 2010).

The V_{S30} database in Taiwan (Kuo et al., 2017) is provided by the National Center for Research of Earthquake Engineering. The database

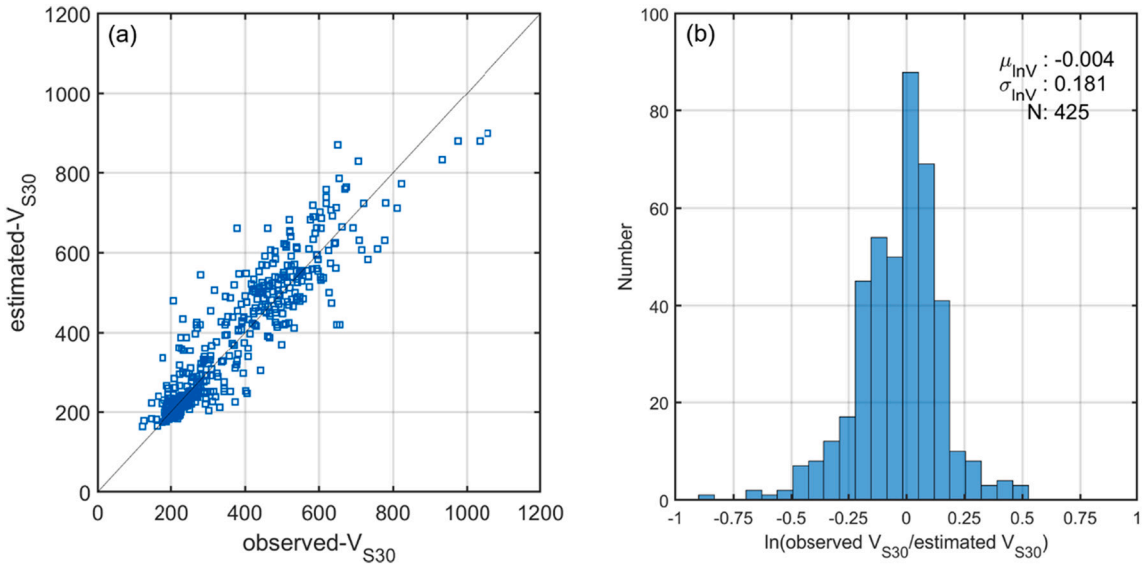

Fig. 6. (a) Comparison of V_{S30} values obtained from EGDT logged data (X axis) with those obtained from MHVSR inversion results in this study (Y axis). (b) Residuals of V_{S30} from estimates based on MHVSR inversion results. μ_{lnV} is the median of the residuals, σ_{lnV} is the standard deviation of the residuals, and N is the number of sites.

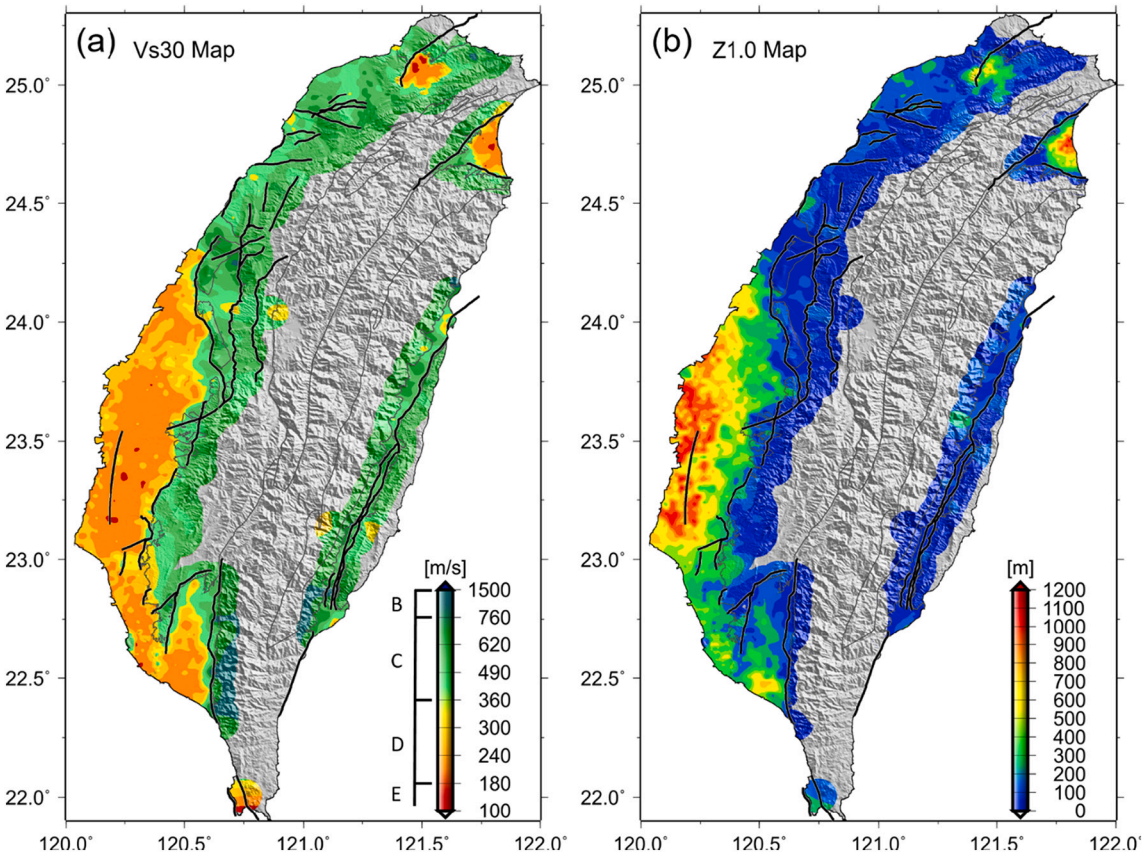

Fig. 7. (a) A dense updated V_{S30} map for Taiwan plains and foothills plotted using 136 microtremor array measurement sites and 3587 MHVSR inversion results. The legend shows the V_{S30} categorized into four soil types based on the National Earthquake Hazards Reduction Program (NEHRP) (FEMA 222A, 1994). (b) The $Z_{1.0}$ map for Taiwan. These maps were plotted using the surface command of generic mapping tools (Wessel and Smith, 1998) considering a 1-km increment and without smoothing.

can also be accessed through the EGDT, which provides V_{S30} information for 816 sites obtained using compound techniques, including suspension PS logging (Kuo et al., 2011, 2012), microtremor array measurements (Kuo et al., 2016), receiver function analysis (Lin et al., 2018), and multiple proxy-based prediction models (Kwok et al., 2018).

The Vs profiles determined using the MHVSR inversion technique were used to calculate V_{S30} according to the following formula:

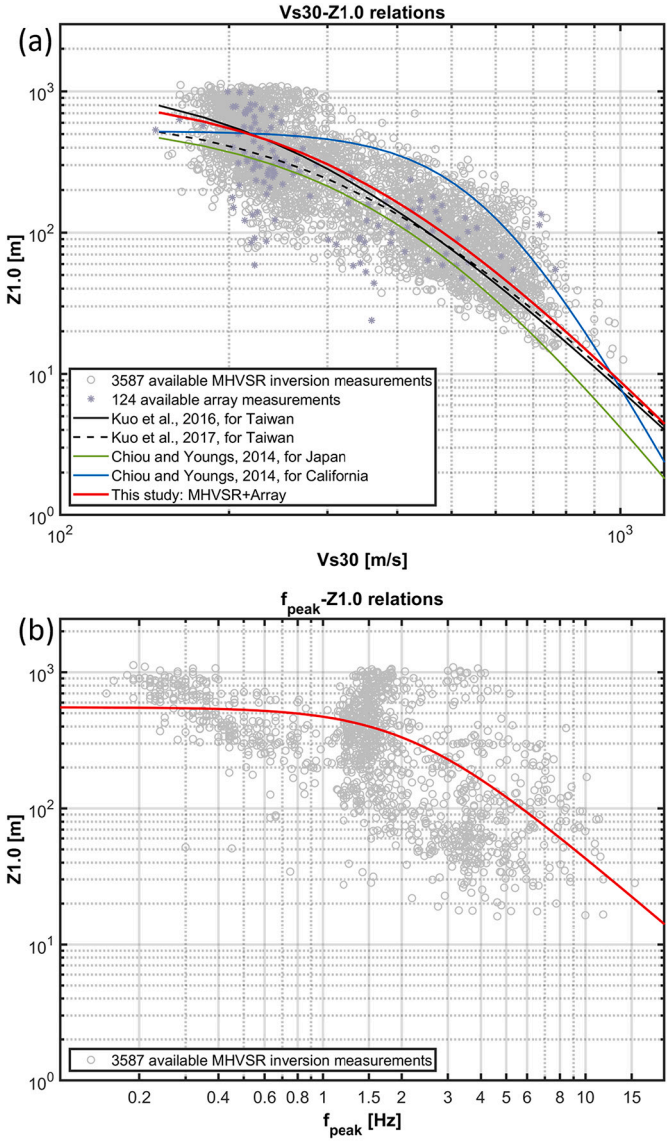

Fig. 8. (a) Distribution of V_{S30} and $Z_{1.0}$ data for 124 microtremor array measurements and 3587 MHVSR inversion results. The V_{S30} – $Z_{1.0}$ relationship is shown, where the green and blue lines demonstrate the relationships for Japan and California, respectively, as determined from the study conducted by Chiou and Youngs (2014), and the black and black dashed lines indicate the relationships for Taiwan, as determined from studies conducted by Kuo et al. (2016) and Kuo et al. (2017), respectively. The V_{S30} – $Z_{1.0}$ relationship developed in this study is indicated by the red line. (b) Distribution of the relationship between f_{peak} and $Z_{1.0}$ for 3587 MHVSR inversion results. The f_{peak} – $Z_{1.0}$ relationship developed in this study is indicated by the red line. (For interpretation of the references to colour in this figure legend, the reader is referred to the web version of this article.)

$$V_{S30} = \frac{30}{\sum_{i=1}^{n}\left(Z_i / Vs_i\right)} \tag{5}$$

where Z_i is the thickness of the i_{th} layer and Vs_i denotes the Vs of the i_{th} layer in a total of n layers existing down to 30 m.

Fig. 6a shows the comparison of V_{S30} determined from the MHVSR inversion results with those obtained from the EGDT. Our inverted V_{S30} were not from the same locations as those from the EGDT. We selected the nearest sites located within 1 km to enable the comparison. The residuals of V_{S30} were calculated using the following formula (Ancheta et al., 2013; Seyhan et al., 2014):

$$R_i = ln\left(Vs30_i^{obs}\right) - ln\left(Vs30_i^{est}\right) \tag{6}$$

where R_i is the residual for site i, $\ln(Vs30_i^{obs})$ is the EGDT V_{S30} for site i, and $\ln(Vs30_i^{est})$ is the inverted V_{S30} for site i. Model bias was estimated from the median of the residuals (μ_{lnV}). The standard deviation of the residuals (σ_{lnV}) was calculated for the entire set of residuals or subsets under certain conditions. The standard deviation represents the divergence of the residuals, and a higher σ_{lnV} indicates that the estimated model has a large uncertainty. The inverted V_{S30} were in agreement with those obtained from the EGDT (Fig. 6b). The μ_{lnV} was low, and σ_{lnV} was only 0.18. These findings demonstrated that the V_{S30} estimated using the MHVSR inversion technique exhibited high reliability. Fig. 7a presents the integration of the V_{S30} map from 136 microtremor array measurement sites and 3587 MHVSR inversion sites. The inversion of Vs profiles in this study enabled us to add more details in the V_{S30} map. In general, V_{S30} values <360 m/s were distributed around the Taipei Basin, Ilan Plain, Yun–Chia–Nan Plain, and Pingtung Plain. Higher V_{S30} values (>360 m/s) were distributed around the Western Foothills Terrane, Huadong Valley, and the mountain foothill area or basin edge.

4.3. Depth contour of $Z_{1.0}$ and relation to V_{S30}

$Z_{1.0}$ is a site parameter defined as a depth where Vs reaches 1 km/s. $Z_{1.0}$ indicates the sedimentary thickness. This parameter has complementarity with V_{S30} and has been widely used in advanced GMPEs (Abrahamson et al., 2014; Boore et al., 2014; Chiou and Youngs, 2014) to represent the thickness of alluvial responses. We used Vs profiles from 124 microtremor array measurements and 3587 MHVSR inversion results to delineate $Z_{1.0}$ depth contours (Fig. 7b). The deepest $Z_{1.0}$ occurred in the Western Plain and Ilan Plain where the maximum depth was approximately 1200 m. For the Western Foothills Terrane, Huadong Valley, and mountain foothill area or basin edge, the $Z_{1.0}$ was typically <200 m.

Because $Z_{1.0}$ is an essential parameter in GMPEs, for specific sites without the $Z_{1.0}$ parameter, a relationship between V_{S30} and $Z_{1.0}$ has been recommended to estimate $Z_{1.0}$ (Abrahamson and Silva, 2008; Chiou and Youngs, 2008, 2014). In this study, we examined the relationship between V_{S30} and $Z_{1.0}$ for Taiwan following the formula proposed by Chiou and Youngs (2014). The dataset included microtremor array and MHVSR inversion results (Fig. 8a). The relationship between V_{S30} and $Z_{1.0}$ for Taiwan was determined as follows:

$$ln(Z_{1.0}) = \frac{-4.15}{2} ln\left(\frac{{V_{S30}}^2 + 334.2^2}{1750^2 + 334.2^2}\right) \tag{7}$$

The relationship between V_{S30} and $Z_{1.0}$ determined in this study is similar to that reported in previous studies conducted in Taiwan (Kuo et al., 2016, 2017). Our model generally agrees with those in previous studies, although our relationship exhibits a higher predicted $Z_{1.0}$ for the same V_{S30} than that in the Japan model (Chiou and Youngs, 2014). This finding indicated that Taiwan has slightly thicker sediments than does Japan. However, our model has a smaller predicted $Z_{1.0}$ for the same V_{S30} than that in the California model (Chiou and Youngs, 2014), indicating that California has significantly thicker sediments than Taiwan. In addition, we plotted the distribution of $Z_{1.0}$ as function of f_{peak}, and proposed an empirical relationship as follows:

$$ln(Z_{1.0}) = \frac{-1.648}{2} ln\left(\frac{{f_{peak}}^2 + 2.166^2}{100^2 + 2.166^2}\right) \tag{8}$$

We found that the scattering of datasets with an f_{peak} of 2–5 Hz was in the order of 1000 m. Hence, we did not observe less scattering in f_{peak} – $Z_{1.0}$ than in V_{S30} – $Z_{1.0}$ in our datasets. The standard deviation of Eq. (8) was 0.81, whereas that of Eq. (7) was 0.51. This finding indicated that the f_{peak} at most sites did not account for the interface of $Z_{1.0}$.

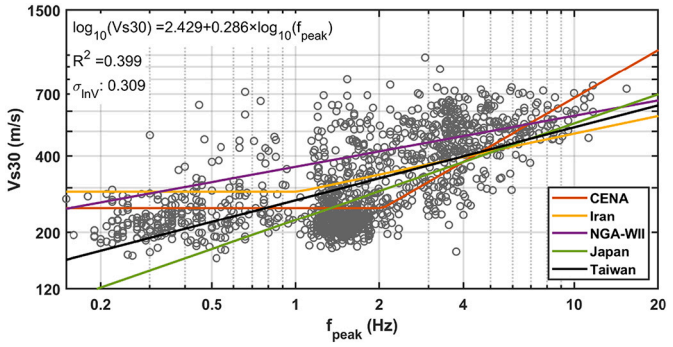

Fig. 9. Distribution of V_{S30} and predominant frequency (f_{peak}) data (gray circles) for 1242 MHVSR sites in Taiwan. Relationships from other regions indicated in different colors. (For interpretation of the references to color in this figure legend, the reader is referred to the web version of this article.)

4.4. Predictive relationship between V_{S30} and MHVSR

The newly developed dense V_{S30} database derived using the MHVSR inversion technique in this study provided not only V_{S30} parameters but also a full 1D Vs structure model with a grid resolution between 1 and 2 km. Although the MHVSR inversion technique is an efficient tool for determining Vs profiles, it is time consuming and requires model validation procedures. For some specific purposes, such as GMPEs, site amplification analysis, and seismic microzonation, determining V_{S30} instead of a full 1D Vs structure is adequate. Hence, we utilized the V_{S30} database obtained in this study to derive a new V_{S30} prediction equation based on MHVSRs and elevation for the rapid evaluation of V_{S30} in Taiwan. To enhance the reliability of the V_{S30} model, we selected only the inverted V_{S30} data with *misfit* < 40 and $R > 0.6$. This allowed us to use 1242 sites for developing the V_{S30} prediction equation.

First, we used the predominant frequency (f_{peak}), V_{S30}, and linear regression analysis to obtain a prediction equation for V_{S30} values using known f_{peak} values:

$$log_{10}(V_{S30}) = 2.429 + 0.286 \times log_{10}(f_{peak}) \tag{9}$$

Fig. 9 reveals the datasets from this study as well as f_{peak}-based V_{S30} prediction models (Eq. (9)) for Taiwan and other regions (Ghofrani and Atkinson, 2014; Hassani and Atkinson, 2016; Yaghmaei-Sabegh and Hassani, 2020).

The standard deviation of the residuals (σ_{lnV}) for the model was 0.31. The coefficient of determination (R^2) for Eq. (9) was 0.399. We compared the prediction model of Taiwan with the other regional f_{peak}-based V_{S30} prediction models developed for California, Japan, and Iran. The σ_{lnV} for the California model (NGA-West2), Japan model (Ghofrani and Atkinson, 2014), Central and Eastern North America model (Hassani and Atkinson, 2016), and Iran model (Yaghmaei-Sabegh and Hassani, 2020) were 0.372, 0.372, 0.322, and 0.223, respectively. Although the residuals representing the f_{peak}-based V_{S30} prediction models were acceptable, they exhibited a large uncertainty. The predominant frequency of the MHVSR or EHVSR correlated with V_{S30}; however, determination of this frequency requires human judgment and is sometimes challenging because of the presence of multiple peaks. Moreover, the examination of the predominant frequency by a human is time consuming and can result in discrepancy. Hence, we defined a new parameter to determine the predictive relationship between the MHVSR and V_{S30}. On the basis of the characteristics of the MHVSR, wherein the amplitude of the predominant frequency typically has a higher value for alluvial sites and the predominant frequency generally tends toward a low value, we present a new parameter, H_R, a relative ratio within the MHVSR as a proxy for V_{S30}. We calculated the ratio between the average MHVSR for the high-frequency ($\overline{HMH}$) and low-frequency ($\overline{HML}$) bands to define H_R. A given central frequency f_c divides the MHVSR into high-

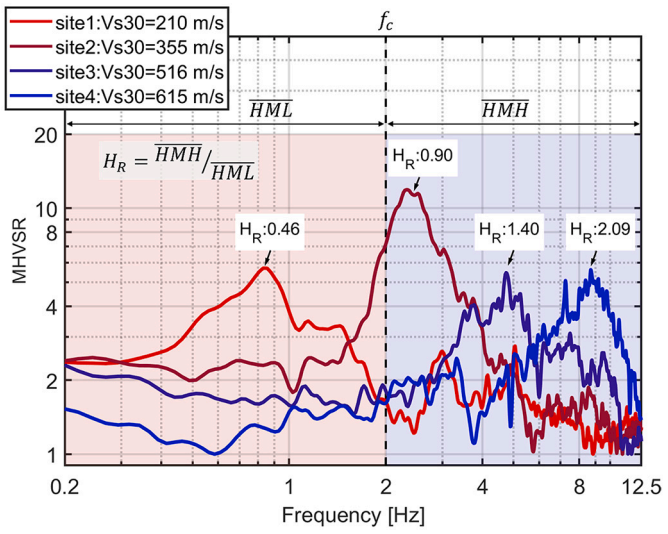

Fig. 10. Schematic of the relationship between MHVSR and H_R. The legend indicates the V_{S30} for each MHVSR site.

frequency and low-frequency bands. H_R is expressed as follows:

$$H_R = \frac{\frac{1}{n}\sum_{i=m+1}^{i=m+n}(\overline{MHVSR})_{fi}}{\frac{1}{m}\sum_{i=1}^{i=m}(\overline{MHVSR})_{fi}} = \frac{\overline{HMH}}{\overline{HML}}, f_m = f_c \tag{10}$$

According to the definition of H_R, the predominant frequency (f_{peak}) dominates the equation for H_R, implying that a high f_{peak} results in a large H_R value (Fig. 10). H_R is considered a relative measurement of the ratio between the amplitude of the site response at high and low frequencies; thus, it is correlated with the predominant resonance frequency, in which a large amplitude ratio exists. A schematic

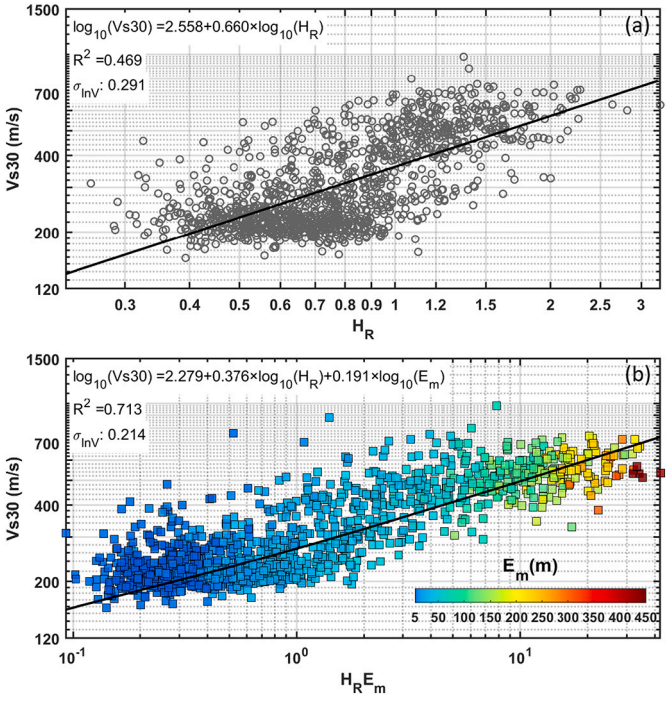

Fig. 11. (a) Variation in estimated V_{S30} from MHVSR inversion versus H_R, represented with gray circles. (b) Variation of estimated V_{S30} from MHVSR inversion versus $H_R E_m$ (represented by squares), where the scattered colors represent modified elevations.

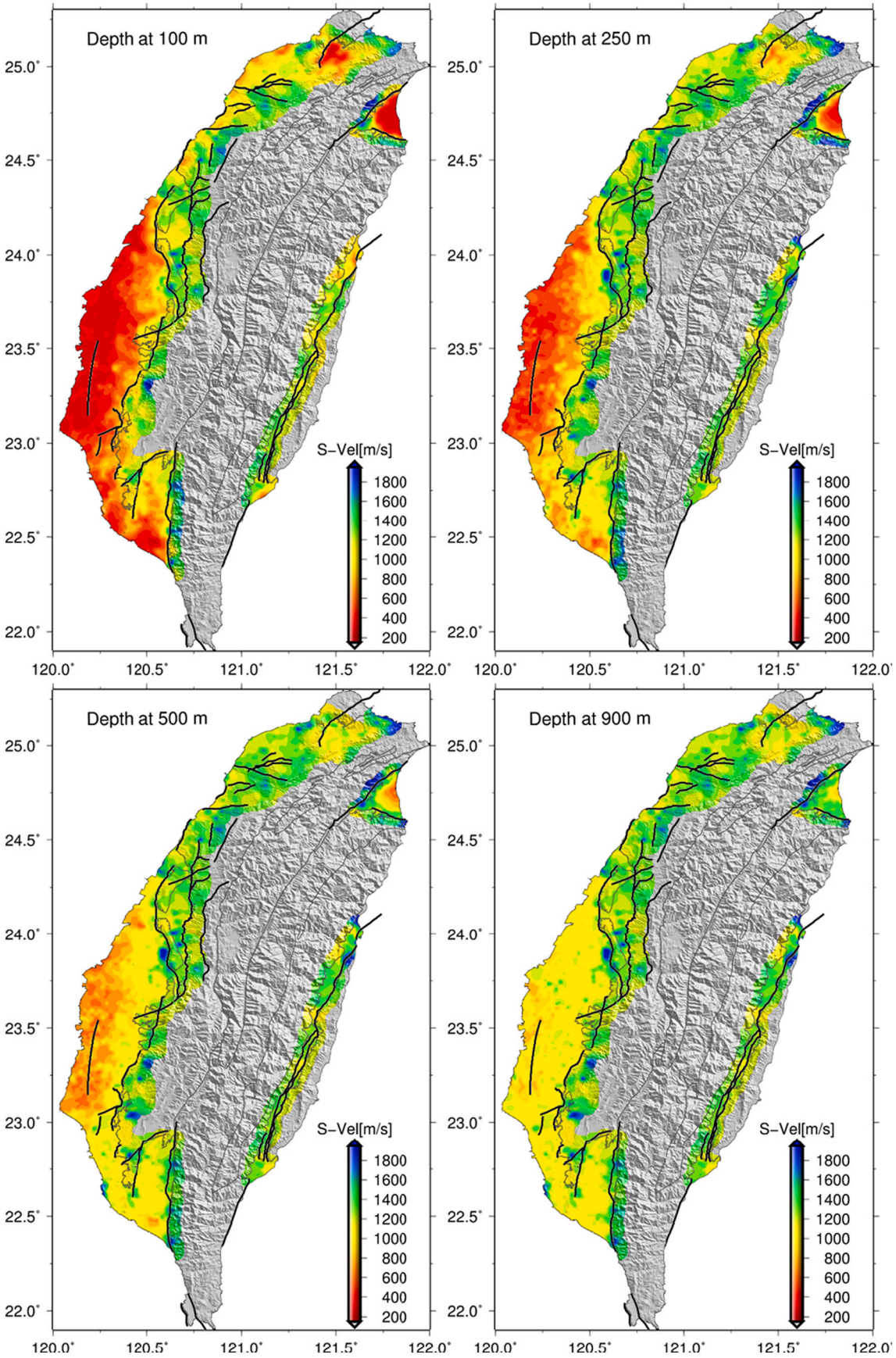

Fig. 12. Comparison of Vs contours at four depth levels (100, 250, 500, and 900 m).

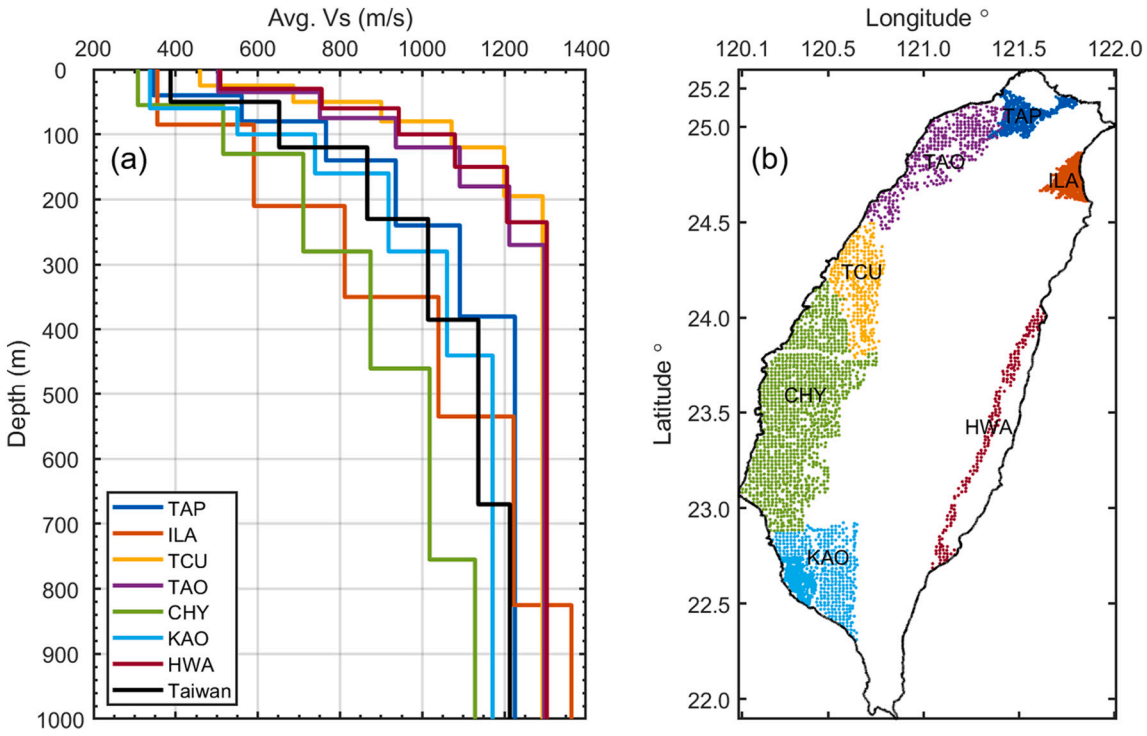

Fig. 13. (a) Average 1D models from all the inverted results in Taiwan overall and in seven areas. (b) Locations of these subareas as well as the abbreviations.

representation of H_R is presented in Fig. 10. When a resonance peak appears at a high frequency (i.e., >2 Hz), $\overline{HMH}$ is larger than $\overline{HML}$, and the value of the resultant H_R is ≥1, as was the case for sites 3 and 4. By contrast, once a resonance peak rises at a low frequency (i.e., <2 Hz), $\overline{HML}$ is larger than $\overline{HMH}$, and the resultant H_R is likely <1, as was the case at site 1. For a resonance peak occurs near the central frequency, the resultant H_R is close to 1, as was the case at site 2. In other words, H_R considers both predominant frequency and amplitude but does not require human judgment and can be calculated automatically. The central frequency f_c plays a crucial role in controlling H_R. In this study, we observed that the optimum value for f_c was 2.0 Hz. This choice is in accordance with the relationship between the predominant frequency and V_{S30} at several regions in previous studies (Hassani and Atkinson, 2016; Yaghmaei-Sabegh and Hassani, 2020). These studies have suggested a transition frequency of 1 or 2 Hz. On the basis of the suggestion, a grid search on f_c was used to minimize the correlation coefficient between H_R and V_{S30}; therefore, we determined 2 Hz as the f_c for Taiwan data. Furthermore, the predominant frequency contour map (Fig. 1b) reveals a 2-Hz contour boundary between the geological structures roughly divided into alluvium and mountain hills. Sedimentary areas thus usually had a predominant frequency of <2 Hz, and the basin edge or foothill areas usually had a predominant frequency of >2 Hz in Taiwan. The f_c could be different in other areas because of substructure or depositional environment variations.

An H_R-based prediction function expressed as follows can be adopted to fit the Taiwan MHVSR inverted V_{S30} database and H_R:

$$log_{10}(V_{S30}) = 2.558 + 0.66 \times log_{10}(H_R) \quad (11)$$

The V_{S30} prediction equation, Eq. (11), is based on the H_R parameter, which resulted in a lower σ_{lnV} value of 0.291 (Fig. 11a) compared with that obtained using f_{peak}. Furthermore, determining the H_R parameter is easier. These results demonstrated that the new parameter H_R is suitable for V_{S30} model predictions.

Geotechnical category and elevation data have been used to infer V_{S30} in Taiwan (Ancheta et al., 2013; Seyhan et al., 2014). Although the topographic slope was well-correlated with V_{S30} (Allen and Wald, 2009; Heath et al., 2020; Wald and Allen, 2007), calculating the topographic slope by using different tools (e.g., generic mapping tools, GMT or ArcGIS) can create inconsistent results (Lemoine et al., 2012). To obtain consistent estimates of the topographic slope, a fixed-resolution DEM and a homogeneous processing procedure should be adopted. To reduce uncertainty in the proxy of V_{S30} by using a simple method, we adopted both H_R and modified elevation as predictor variables in this study to regress a predicted equation as follows:

$$log_{10}(V_{S30}) = 2.279 + 0.376 \times log_{10}(H_R) + 0.191 \times log_{10}(E_m) \quad (12)$$

where E_m denotes the modified elevation, which fixes elevations below 5 m to be equal to 5 m. Using Eq. (12), the uncertainty in the predicted V_{S30} could be considerably decreased to 0.214 (Fig. 11b). The coefficients of determination (R^2) for Eqs. (11) and (12) were 0.469 and 0.713, respectively. The p values of both the independent variables were <0.05 in the partial F test; thus, both $log_{10}(H_R)$ and $log_{10}(E_m)$ were significant parameters in Eq. (12). According to the success of the proposed V_{S30} prediction equation, this study demonstrated the ability of a new V_{S30} proxy and revealed the reliability of our inverted V_{S30} database.

4.5. 3D shallow Vs model in Taiwan

Distinct inverted 1D models obtained from the MHVSR and microtremor arrays at different locations were used to construct the Taiwan pseudo-3D shallow Vs model (TSVM) in the plain areas of Taiwan. All 1D Vs profiles were assembled into pseudo-3D models by using an inverse distance weighted interpolation by employing MATLAB software. Fig. 12 presents Vs contours at four depth levels (100, 250, 500, and 900 m). The clear geological structure boundary could be identified from the lateral distribution of velocities. In general, at depths of 100 and 250 m, the Taipei Basin, Ilan Plain, and Yun–Chia–Nan Plain presented lower distributed velocities than did the Western Foothills Terrane and Huadong Valley. The velocity contrast was lower at depths of >500 m than that in shallow parts; however, the velocities distributed in the Western Foothills Terrane and Huadong Valley were still higher than those in other areas. The velocity model's lateral distribution exhibited similar

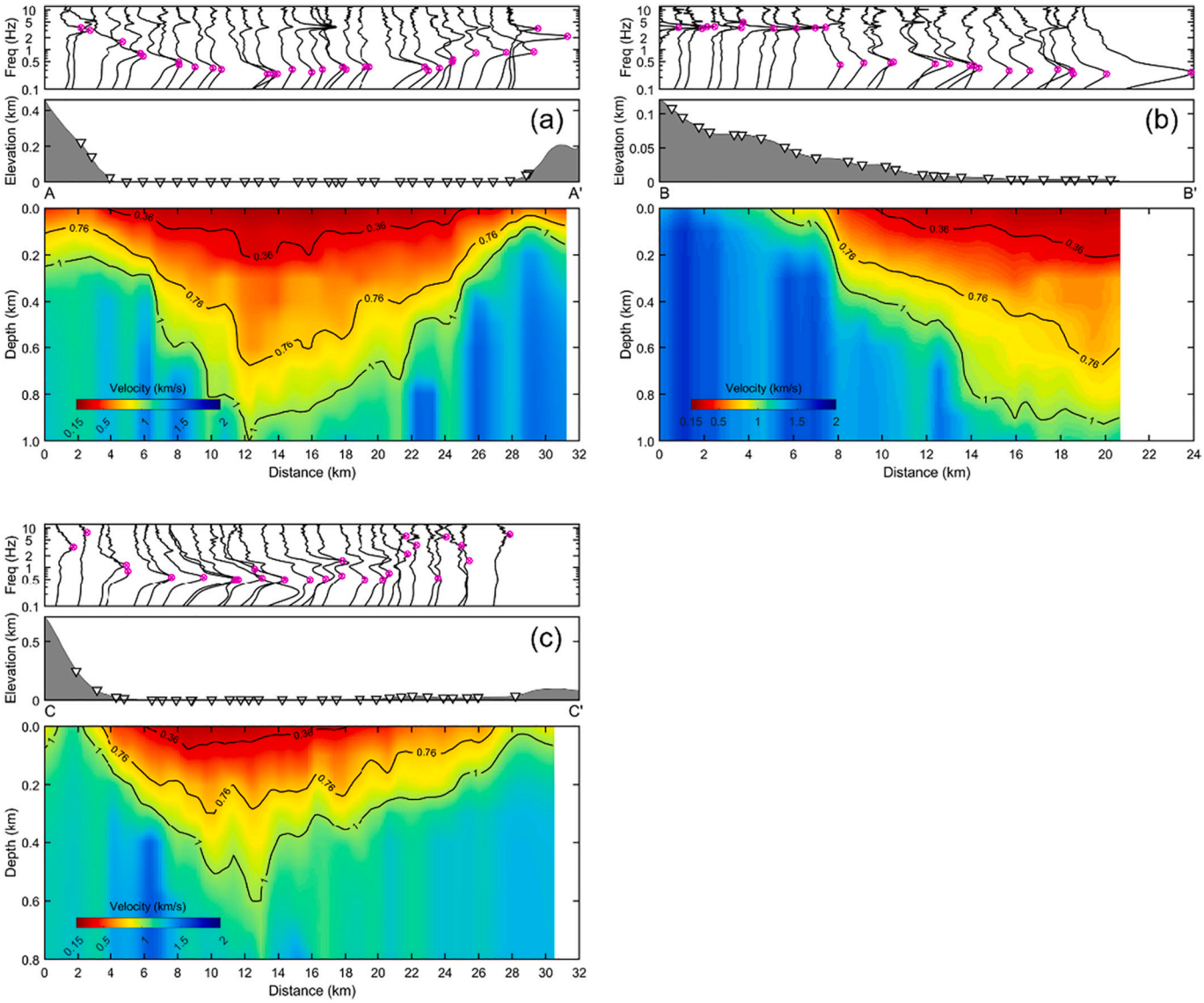

Fig. 14. The three cross-sections of the inverted 3D Vs model. The location of these sections are indicated in Fig. 1b. The top panel of each figure is the MHVSR, highlighting the predominant frequency; the middle panel is the station location with the topography; the bottom panel is the Vs model slice along the section. (a) The A–A′ cross-section cuts north to south along the coast of the Ilan Plain. (b) The B–B′ cross-section cuts southwest to northeast across the Ilan Plain. (c) The C–C′ cross-section cuts north to south across the Taipei Basin.

patterns as did the MHVSR predominant frequency (Fig. 1b), where low-velocity distribution corresponded to a low predominant frequency (<2 Hz). The Taipei Basin, Ilan Plain, Pingtung Plain, and Yun–Chia–Nan Plain had lower predominant frequencies than did the Western Foothills Terrane and Huadong Valley.

The 1D average Vs model for the entire Taiwan as well as the 1D average Vs models of seven areas are presented in Fig. 13a. The locations of these areas as well as the abbreviations are indicated in Fig. 13b. Each Vs model was averaged from all Vs profiles in an area. The Vs profiles were sliced into 5-m layers, and the mean was calculated to obtain the 1D Vs model. On the basis of gradient changes in velocity structures, we restratified them into six layers as a simplified model. Thus, the 1D models for different areas exhibited distinct thicknesses. The variation in near-surface lateral velocity was significant for certain areas. The Yun–Chia–Nan Plain (CHY) and the Ilan Plain (ILA) had the lowest average velocities in Taiwan, which could be related to thicker unconsolidated sediments.

Fig. 14 presents three cross-sections along the Taipei Basin and Ilan Plain from the TSVM. The location of these sections are indicated in Fig. 1b. The elevation along the profiles and MHVSRs with predominant frequency highlighted were plotted in each cross-section. The A–A′ cross-section cuts north to south along the coast of the Ilan Plain. The sediment thickness varied from thin to thick to thin again in this cross-section. The sediment thickness (covering bedrock with Vs $\geq$ 760 m/s) ranged from 50 m to approximately 700 m. The B–B′ cross-section cuts southwest to northeast through the Ilan Plain. This profile crosses the mountain hill area to the coastline area, and the sediment thickness exhibited more lateral variations ranging from 0 m to approximately 700 m. The deepest parts of the sediment were located in the center and near the coastline. The C–C′ profile crosses the Taipei Basin north to south. The thicker sediment was located in the center of the basin, and the basin edge had relatively thin sediment and high velocity. The Vs distribution is consistent with the topography of the three cross-sections and is associated with the predominant frequency of the MHVSR. In the top panel of each figure, the MHVSR peaks corresponded to sediment thickness. A low MHVSR predominant frequency had lower Vs and deeper sediment distribution, and the high MHVSR predominant frequency had higher Vs and thinner sediment distribution. Our model

agrees with the results of previous studies in the Taipei Basin (Wang et al., 2004) and the Ilan Plain (Shi, 2011), indicating that the results of MHVSR inversion not only fit the shallow Vs distribution but also have the ability to reveal the stratum interface.

5. Conclusions

Using DFA theory and the computer code HV-inv, we inverted 3587 MHVSRs in Taiwan to obtain Vs profiles. The obtained 1D velocity results were used to calculate the site parameters V_{S30} and $Z_{1.0}$. The site parameter data provide a denser and higher spatial resolution with respect to previous studies, thus indicating the importance of site amplification investigation and providing valuable information for reducing seismic hazards. We proposed new V_{S30} predictive equations and introduced a new parameter, H_R, which is defined as a ratio of the amplitude of the MHVSR between high and low frequency; this parameter is proportional to a predominant frequency without subjective selection. Our H_R-based V_{S30} proxy model reduced the standard deviation of V_{S30} estimates, thus outperforming the f_{peak}-based proxy. Notably, when E_m was used in the H_R-based model, the standard deviation in V_{S30} predictions was further reduced. When the MHVSR and elevation are both available, we suggest H_R and E_m as optimal parameters as V_{S30} proxies in Taiwan. We constructed the TSVM that described main shallow structural features with unprecedented detail in the plain areas of Taiwan. This study contributes to 3D seismic wave simulations and ground motion predictions with higher resolution and accuracy. In this study, dense inverted 1D Vs models were derived only for the plain and foothill areas; thus, studies investigating mountain areas are still lacking. The MHVSR technique may have limitations in areas with complex or oblique underground structures. The highly complex geological structures in mountain areas require further investigation and new techniques for accurate surveying.

Author statement

All authors participated in the interpretation of data and discussion of the results.

Declaration of Competing Interest

This work is supported by the Ministry of Science and Technology of Taiwan. The authors declare there is no conflicts of interest.

Acknowledgments

We thank Dr. Hsin-Hua Huang for the helpful discussion. We thank two anonymous reviewers for valuable and constructive comments helping improve this article. Logging data were obtained from the EGDT for the TSMIP (http://egdt.ncree.org.tw, last accessed May 2019). This work was funded by the Ministry of Science and Technology (MOST 109-2811-M-001-552 and MOST 109-2116-M-492-002) and supported by the Taiwan Earthquake Research Center (contribution number 00173). The corresponding author also acknowledges the support by National Central University through the project number 110A1113-3.

References

Abrahamson, N., Silva, W., 2008. Summary of the Abrahamson & Silva NGA ground-motion relations. Earthquake Spectra 24, 67–97. https://doi.org/10.1193/1.2924360.

Abrahamson, N.A., Silva, W.J., Kamai, R., 2014. Summary of the ASK14 ground motion relation for active crustal regions. Earthquake Spectra 30, 1025–1055. https://doi.org/10.1193/070913EQS198M.

Allen, T.I., Wald, D.J., 2009. On the use of high-resolution topographic data as a proxy for seismic site conditions (V_{S30}). Bulletin of the Seismological Society of America 99, 935–943. https://doi.org/10.1785/0120080255.

Ancheta, T.D., Darragh, R.B., Stewart, J.P., Seyhan, E., Silva, W.J., Chiou, B.S., Wooddell, K.E., Graves, R.W., Kottke, A.R., Boore, D.M., 2013. Peer NGA-West 2 database. In: PEER Report No. 2013/2003. Pacific Earthquake Engineering Research Center, University of California, Berkeley, CA, 2134 pp.

ASCE, 2010. Minimum Design Loads for Buildings and Other Structures (ASCE/SEI 7–10). Structural Engineering Institute, American Society of Civil Engineering, Reston, Virginia.

Boore, D.M., Stewart, J.P., Seyhan, E., Atkinson, G.M., 2014. NGA-West2 equations for predicting PGA, PGV, and 5% damped PSA for shallow crustal earthquakes. Earthquake Spectra 30, 1057–1085. https://doi.org/10.1193/070113EQS184M.

BSSC, 2004. NEHRP Recommended Provisions for Seismic Regulations for New Buildings and Other Structures (FEMA 450), Part 1. Provisions; Part 2. Commentary. Building Seismic Safety Council for the Federal Emergency Management Agency.

Capon, J., 1969. High-resolution frequency-wavenumber spectrum analysis. Proc. IEEE 57, 1408–1418. https://doi.org/10.1109/PROC.1969.7278.

Castellaro, S., 2016. The complementarity of H/V and dispersion curves. Geophysics 81, T323–T338. https://doi.org/10.1190/geo2015-0399.1.

Chan, C.-H., Ma, K.-F., Shyu, J.B.H., Lee, Y.-T., Wang, Y.-J., Gao, J.-C., Yen, Y.-T., Rau, R.-J., 2020. Probabilistic seismic hazard assessment for Taiwan: TEM PSHA2020. Earthquake Spectra 36, 137–159. https://doi.org/10.1177/8755293020951587.

Chen, C.-T., Kuo, C.-H., Wen, K.-L., Lin, C.-M., Huang, J.-Y., 2016. Simulating Shallow Soil Response using Wave Propagation Numerical Modelling in the Western Plain of Taiwan. TAO: Terrestrial, Atmospheric and Oceanic Sciences 27, 359. https://doi.org/10.3319/TAO.2016.01.06.01(TEM).

Chiou, B.S.-J., Youngs, R.R., 2008. An NGA model for the average horizontal component of peak ground motion and response spectra. Earthquake Spectra 24, 173–215. https://doi.org/10.1193/1.2894832.

Chiou, B.S.-J., Youngs, R.R., 2014. Update of the Chiou and Youngs NGA model for the average horizontal component of peak ground motion and response spectra. Earthquake Spectra 30, 1117–1153. https://doi.org/10.1193/072813EQS219M.

FEMA 222A, 1994. NEHRP Recommended Provisions for the Development of Seismic Regulations for New Buildings, 1994 Edition, Part 1 — Provisions. Federal Emergency Management Agency, 290 pp.

García-Jerez, A., Luzón, F., Sánchez-Sesma, F.J., Lunedei, E., Albarello, D., Santoyo, M. A., Almendros, J., 2013. Diffuse elastic wavefield within a simple crustal model. Some consequences for low and high frequencies. Journal of Geophysical Research: Solid Earth 118, 5577–5595. https://doi.org/10.1002/2013jb010107.

García-Jerez, A., Piña-Flores, J., Sánchez-Sesma, F.J., Luzón, F., Perton, M., 2016. A computer code for forward calculation and inversion of the H/V spectral ratio under the diffuse field assumption. Comput. Geosci. 97, 67–78. https://doi.org/10.1016/j.cageo.2016.06.016.

García-Jerez, A., Seivane, H., Navarro, M., Martínez-Segura, M., Piña-Flores, J., 2019. Joint analysis of Rayleigh-wave dispersion curves and diffuse-field HVSR for site characterization: the case of El Ejido town (SE Spain). Soil Dyn. Earthq. Eng. 121, 102–120. https://doi.org/10.1016/j.soildyn.2019.02.023.

Ghofrani, H., Atkinson, G.M., 2014. Site condition evaluation using horizontal-to-vertical response spectral ratios of earthquakes in the NGA-West 2 and Japanese databases. Soil Dyn. Earthq. Eng. 67, 30–43. https://doi.org/10.1016/j.soildyn.2014.08.015.

Goldberg, D.E., 1989. Genetic Algorithms in Search, Optimization and Machine Learning. Reading, MA, Addison Wesley.

Guéguen, P., Chatelain, J.-L., Guillier, B., Yepes, H., Egred, J., 1998. Site effect and damage distribution in Pujili (Ecuador) after the 28 March 1996 earthquake. Soil Dyn. Earthq. Eng. 17, 329–334. https://doi.org/10.1016/S0267-7261(98)00019-0.

Hassani, B., Atkinson, G.M., 2016. Applicability of the site fundamental frequency as a V_{S30} proxy for central and eastern North America. Bull. Seismol. Soc. Am. 106, 653–664. https://doi.org/10.1785/0120150259.

Heath, D.C., Wald, D.J., Worden, C.B., Thompson, E.M., Smoczyk, G.M., 2020. A global hybrid V_{S30} map with a topographic slope–based default and regional map insets. Earthquake Spectra 0. https://doi.org/10.1177/8755293020911137, 8755293020911137.

Herrmann, R., 1987. Computer Programs in Seismology. Saint Louis University, St. Louis, MO.

Horike, M., 1985. Inversion of phase velocity of long-period microtremors to the S-wave-velocity structure down to the basement in urbanized areas. Journal of Physics of the Earth 33, 59–96. https://doi.org/10.4294/jpe1952.33.59.

Huang, H.-C., Wu, C.-F., 2006. Estimations of the S-wave velocity structures in Chia-Yi City, Taiwan, using the array records of microtremors. Earth, planets and space 58, 1455–1462. https://doi.org/10.1186/BF03352644.

Huang, H.-C., Wu, C.-F., Lee, F.-M., Hwang, R.-D., 2015. S-wave velocity structures of the Taipei Basin, Taiwan, using microtremor array measurements. J. Asian Earth Sci. 101, 1–13. https://doi.org/10.1016/j.jseaes.2015.01.003.

Kaneko, F., Kanemori, T., Tonouchi, K., 1990. Low-Frequency Shear Wave Logging in Unconsolidated Formations for Geotechnical applications. In: Paillet, F.L., Saunders, W.R. (Eds.), ASTM International. West Conshohocken, PA, pp. 79–98.

Karagoz, O., Chimoto, K., Citak, S., Ozel, O., Yamanaka, H., Hatayama, K., 2015. Estimation of shallow S-wave velocity structure and site response characteristics by microtremor array measurements in Tekirdag region, NW Turkey. Earth, Planets and Space 67, 1–17. https://doi.org/10.1186/s40623-015-0320-1.

Kawase, H., Sánchez-Sesma, F.J., Matsushima, S., 2011. The optimal use of horizontal-to-vertical spectral ratios of earthquake motions for velocity inversions based on diffuse-field theory for plane waves. Bull. Seismol. Soc. Am. 101, 2001–2014. https://doi.org/10.1785/0120100263.

Kuo, C.-H., 2004. Shallow S-Wave Velocity Structure of some Strong Motion Stations in Different Geological Areas (Master's Thesis). National Central University, Taoyuan.

Kuo, C.-H., Cheng, D.-S., Hsieh, H.-H., Chang, T.-M., Chiang, H.-J., Lin, C.-M., Wen, K.-L., 2009. Comparison of three different methods in investigating shallow shear-wave

velocity structures in Ilan, Taiwan. Soil Dynamics and Earthquake Engineering 29, 133–143. https://doi.org/10.1016/j.soildyn.2008.01.010.
Kuo, C.-H., Wen, K.-L., Hsieh, H.-H., Chang, T.-M., Lin, C.-M., Chen, C.-T., 2011. Evaluating empirical regression equations for Vs and estimating V_{S30} in northeastern Taiwan. Soil Dynamics and Earthquake Engineering 31, 431–439. https://doi.org/10.1016/j.soildyn.2010.09.012.
Kuo, C.-H., Wen, K.-L., Hsieh, H.-H., Lin, C.-M., Chang, T.-M., Kuo, K.-W., 2012. Site classification and V_{S30} estimation of free-field TSMIP stations using the logging data of EGDT. Engineering Geology 129, 68–75. https://doi.org/10.1016/j.enggeo.2012.01.013.
Kuo, C.-H., Chen, C.-T., Lin, C.-M., Wen, K.-L., Huang, J.-Y., Chang, S.-C., 2016. S-wave velocity structure and site effect parameters derived from microtremor arrays in the Western Plain of Taiwan. J. Asian Earth Sci. 128, 27–41. https://doi.org/10.1016/j.jseaes.2016.07.012.
Kuo, C.-H., Lin, C.-M., Chang, S.-C., Wen, K.-L., Hsieh, H.-H., 2017. Site database for Taiwan strong motion stations. In: Technical Report of National Center for Research on Earthquake Engineering, NCREE-17-004.
Kwok, O.L.A., Stewart, J.P., Kwak, D.Y., Sun, P.-L., 2018. Taiwan-specific model for V_{S30} prediction considering between-proxy correlations. Earthquake Spectra 34, 1973–1993. https://doi.org/10.1193/061217EQS113M.
Lee, S.-J., Chen, H.-W., Huang, B.-S., 2008. Simulations of strong ground motion and 3D amplification effect in the Taipei Basin by using a composite grid finite-difference method. Bull. Seismol. Soc. Am. 98, 1229–1242. https://doi.org/10.1785/0120060098.
Lemoine, A., Douglas, J., Cotton, F., 2012. Testing the applicability of correlations between topographic slope and V_{S30} for Europe. Bulletin of the Seismological Society of America 102, 2585–2599. https://doi.org/10.1785/0120110240.
Lin, C.-M., Chang, T.-M., Huang, Y.-C., Chiang, H.-J., Kuo, C.-H., Wen, K.-L., 2009. Shallow S-wave velocity structures in the western coastal plain of Taiwan. Terrestrial, Atmospheric & Oceanic Sciences 20. https://doi.org/10.3319/TAO.2007.12.10.01(T).
Lin, C.-M., Kuo, C.-H., Huang, J.-Y., Hsieh, H.-H., Si, C.-C., Wen, K.-L., 2018. Shallow Shear-Wave Velocity Structures of TSMIP Stations in Taiwan. NCREE Report no. NCREE-18-019. National Center for Research, Taipei, Taiwan.
Matsushima, T., Okada, H., 1990. Determination of deep geological structures under urban areas using long-period microtremors. Butsuri-Tansa 43, 21–33.
Miksat, J., Wen, K.-L., Sokolov, V., Chen, C.-T., Wenzel, F., 2010. Simulating the Taipei basin response by numerical modeling of wave propagation. Bull. Earthq. Eng. 8, 847–858. https://doi.org/10.1007/s10518-009-9171-0.
Nakamura, Y., 1989. A Method for Dynamic Characteristics Estimation of Subsurface Using Microtremor on the Ground Surface. Railway Technical Research Institute, p. 30. Quarterly Reports.
Nakamura, Y., 2019. What is the Nakamura method? Seismol. Res. Lett. 90, 1437–1443. https://doi.org/10.1785/0220180376.
Nazarian, S., Stokoe II, K.H., Hudson, W.R., 1983. Use of Spectral Analysis of Surface Waves Method for Determination of Moduli and Thicknesses of Pavement Systems.
Ogura, K., 1988. Expansion of applicability for suspensor PS logging. In: OYO Technical Roport, pp. 69–98.
Panou, A.A., Theodulidis, N., Hatzidimitriou, P., Stylianidis, K., Papazachos, C.B., 2005. Ambient noise horizontal-to-vertical spectral ratio in site effects estimation and correlation with seismic damage distribution in urban environment: the case of the city of Thessaloniki (Northern Greece). Soil Dyn. Earthq. Eng. 25, 261–274. https://doi.org/10.1016/j.soildyn.2005.02.004.
Park, C.B., Miller, R.D., Xia, J., 1999. Multichannel analysis of surface waves. Geophysics 64, 800–808. https://doi.org/10.1190/1.1444590.
Picozzi, M., Parolai, S., Richwalski, S., 2005. Joint inversion of H/V ratios and dispersion curves from seismic noise: estimating the S-wave velocity of bedrock. Geophys. Res. Lett. 32 https://doi.org/10.1029/2005GL022878.
Piña-Flores, J., Perton, M., García-Jerez, A., Carmona, E., Luzón, F., Molina-Villegas, J. C., Sánchez-Sesma, F.J., 2017. The inversion of spectral ratio H/V in a layered system using the diffuse field assumption (DFA). Geophys. J. Int. 208, 577–588. https://doi.org/10.1093/gji/ggw416.
Sánchez-Sesma, F.J., Rodríguez, M., Iturrarán-Viveros, U., Luzón, F., Campillo, M., Margerin, L., García-Jerez, A., Suarez, M., Santoyo, M.A., Rodríguez-Castellanos, A., 2011. A theory for microtremor H/V spectral ratio: application for a layered medium. Geophys. J. Int. 186, 221–225. https://doi.org/10.1111/j.1365-246X.2011.05064.x.
Satoh, T., Kawase, H., Iwata, T., Higashi, S., Sato, T., Irikura, K., Huang, H.-C., 2001. S-Wave velocity structure of the Taichung Basin, Taiwan, estimated from array and single-station records of microtremors. Bull. Seismol. Soc. Am. 91, 1267–1282. https://doi.org/10.1785/0120000706.
Senna, S., Wakai, A., Suzuki, H., Yatagai, A., Matsuyama, H., Fujiwara, H., 2018. Modeling of the subsurface structure from the seismic bedrock to the ground surface for a broadband strong motion evaluation in Kumamoto Plain. Journal of Disaster Research 13 (5), 917–927.
Seyhan, E., Stewart, J.P., Ancheta, T.D., Darragh, R.B., Graves, R.W., 2014. NGA-West2 site database. Earthquake Spectra 30, 1007–1024. https://doi.org/10.1193/062913EQS180M.
Shi, Z.-W., 2011. Investigating the Basement Depth and Tectonic Evolution in Ilan Plain by Seismic Reflection Method (Master's Thesis). National Central University, Taoyuan.
Shyu, J.B.H., Chuang, Y.-R., Chen, Y.-L., Lee, Y.-R., Cheng, C.-T., 2016. A new on-land seismogenic structure source database from the Taiwan Earthquake Model (TEM) project for seismic hazard analysis of Taiwan. Terrestrial, Atmospheric & Oceanic Sciences 27. https://doi.org/10.3319/TAO.2015.11.27.02(TEM).
Singh, S.K., Mena, E.A., Castro, R., 1988. Some aspects of source characteristics of the 19 September 1985 Michoacan earthquake and ground motion amplification in and near Mexico City from strong motion data. Bull. Seismol. Soc. Am. 78, 451–477.
Sivaram, K., Gupta, S., Kumar, S., Prasad, B., 2018. Shear velocity structural characterization around the Lonar crater using joint inversion of ambient noise HVSR and Rayleigh wave dispersion. J. Appl. Geophys. 159, 773–784. https://doi.org/10.1016/j.jappgeo.2018.10.022.
Spica, Z., Perton, M., Nakata, N., Liu, X., Beroza, G.C., 2018. Shallow VS imaging of the Groningen area from joint inversion of multimode surface waves and H/V spectral ratios. Seismol. Res. Lett. 89, 1720–1729. https://doi.org/10.1785/0220180060.
Tokimatsu, K., Shinzawa, K., Kuwayama, S., 1992. Use of short-period microtremors for VS profiling. J. Geotech. Eng. 118, 1544–1558. https://doi.org/10.1061/(ASCE)0733-9410(1992)118:10(1544).
Wald, D.J., Allen, T.I., 2007. Topographic slope as a proxy for seismic site conditions and amplification. Bull. Seismol. Soc. Am. 97, 1379–1395. https://doi.org/10.1785/0120060267.
Wang, C.-Y., Lee, Y.-H., Ger, M.-L., Chen, Y.-L., 2004. Investigating subsurface structures and P-and S-wave velocities in the Taipei basin. Terrestrial Atmospheric and Oceanic Sciences 15, 609–628. https://doi.org/10.3319/TAO.2004.15.4.609(T).
Wang, Y.-J., Chan, C.-H., Lee, Y.-T., Ma, K.-F., Shyu, J.B.H., Rau, R.-J., Cheng, C.-T., 2016. Probabilistic Seismic Hazard Assessment for Taiwan. TAO: Terrestrial, Atmospheric and Oceanic Sciences 27, 325. https://doi.org/10.3319/TAO.2016.05.03.01(TEM).
Wen, K.-L., Huang, J.-Y., 2012. Dense microtremor survey for site effect study in Taiwan. In: Proceedings of the 15th World Conference of Earthquake Engineering (15WCEE), pp. 24–28.
Wessel, P., Smith, W.H., 1998. New, improved version of Generic Mapping Tools released. Eos, Transactions American Geophysical Union 79 (47), 579.
Wu, C.-F., Huang, H.-C., 2012. Estimation of shallow S-wave velocity structure in the Puli basin, Taiwan, using array measurements of microtremors. Earth, Planets and Space 64, 389–403.
Wu, C.-F., Huang, H.-C., 2013. Near-surface shear-wave velocity structure of the Chiayi Area, Taiwan. Bulletin of the Seismological Society of America 103, 1154–1164.
Yaghmaei-Sabegh, S., Hassani, B., 2020. Investigation of the relation between V_{S30} and site characteristics of Iran based on horizontal-to-vertical spectral ratios. Soil Dynamics and Earthquake Engineering 128, 105899.
Yamada, M., Cho, I., Kuo, C.-H., Lin, C.-M., Miyakoshi, K., Guo, Y., Hayashida, T., Matsumoto, Y., Mori, J., Yen, Y.-T., Kuo, K.-C., 2020. Shallow subsurface structure in Hualien basin and the relevance to the damage pattern and fault rupture during the 2018 Hualien earthquake. Bulletin of Seismological Society of America 110 (6), 2939–2952.
Yilar, E., Baise, L.G., Ebel, J.E., 2017. Using H/V measurements to determine depth to bedrock and V_{S30} in Boston, Massachusetts. Engineering Geology 217, 12–22.